ESCI-555 Lecture Notes: Parameterized Convection

Helge M. Gonnermann, *Earth, Environmental and Planetary Sciences, Rice University*

1. THERMAL CONVECTION

1.1. Introduction

Imaging hitching a ride with a parcel of fluid within a body of fluid that is heated from below and cooled from above:

heating → expansion → rise → cooling → contraction → sink

The corresponding conceptual model is a layer of fluid heated from below and cooled from above, so that there is a temperature difference of ΔT across the layer and at steady state the heat conducted across the bottom and top boundaries is equal and given by the heat flux q. The fundamental concept is that convection is characterized by temperature fluctuations at the macroscopic scale.

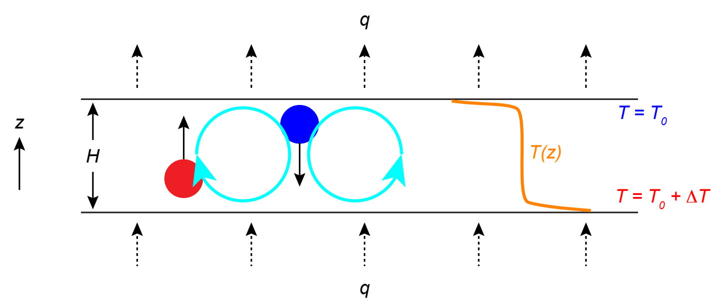

Figure 1

Conceptual model for Rayleigh-Benard convection. A fluid layer of thickness H is heated from below and cooled from above, by maintaining a temperature difference across the layer of ΔT. At steady stead the heat flux across the bottom and top boundaries, q, is the same. A spherical blobs shown in red (blue) of hot (cold) and buoyantly rising (sinking) indicates the convective motions of the fluid. The cyan-colored circles with arrows indicate the overall convective motions after the onset of convection. The length scales over which convective velocities change is H, as is the length scale of temperature changes that scale as ΔT. The temperature profile shown in orange indicates the formation of hot and cold thermal boundary layers.

The following analysis pertains to conditions where the viscous force is dominant over inertial forces, as is the case for Earth's mantle. In this case the viscous force is balanced by the buoyancy force

$$\left|\mu\nabla^2\mathbf{u}\right| \sim \left|\mathbf{g}\rho\gamma\Delta T\right|, \qquad 1.$$

or equivalently

$$\left|\nu\nabla^2\mathbf{u}\right| \sim \left|\mathbf{g}\gamma\Delta T\right|. \qquad 2.$$

Here μ is the dynamic viscosity, $\nu = \mu/\rho$ is the kinematic viscosity, ρ is the density of the fluid, $\mathbf{u}$ is the fluid velocity, $\mathbf{g}$ is the acceleration due to gravity, γ is the thermal expansivity, T is temperature and ΔT is the difference in temperature between bottom and top of the fluid layer.

Using H as the characteristic length scale, and U as the characteristic velocity scale, we can non-dimensionalize the force balance to obtain

$$U \sim \frac{g\gamma\Delta T H^2}{\nu}. \qquad 3.$$

The characteristic time scale for buoyant rise across the layer is given by

$$\tau_U \sim H/U. \tag{4.}$$

As hot or cold fluid traverses the fluid layer, it loses heat to the surrounding fluid by conduction. For convection to occur temperature variations of the order of ΔT have to persist across the entire thickness of the layer, we define the characteristic diffusion time scale, τ_α using the layer thickness, H, and the thermal diffusivity, α, to obtain

$$\tau_\alpha \sim H^2/\alpha. \tag{5.}$$

For convective motions to occur $\tau_\alpha \gg \tau_U$, or

$$1 \ll \frac{\tau_\alpha}{\tau_U} = \frac{g\gamma\Delta T H^3}{\alpha\nu} \equiv \mathrm{Ra}, \tag{6.}$$

where the term on the right hand side of this equation is called the *Rayleigh number*. It is found that if Ra is greater than some critical value, $\mathrm{Ra}_c \approx 1000$, the fluid layer will convect.

SUMMARY POINTS

1. At small Rayleigh numbers (but above the critical Ra), convection in a layer of uniform thickness takes the form of rolls and hexagonal cells.
2. At high Rayleigh numbers heat is *conducted* across (thin) thermal boundary layers at the heated bottom and/or cooled top. The thermal boundary are in a perpetual state of critical instability, giving rise to *thermally buoyant plumes*.
3. During high Ra convection, heat is *advected* by plumes across the interior and the interior temperature is *on average* uniform (adiabatic).
4. If viscosity is temperature dependent it affects the cold thermal boundary layer, which can become a *sluggish lid* or a *stagnant lid*.
   - At viscosity contrasts of <100 the upper boundary is entirely mobile.
   - At viscosity contrasts of 10^2 to 10^3 the upper boundary becomes sluggish (sluggish lid).
   - At viscosity contrasts of 10^4 the upper boundary becomes stagnant (stagnant lid).
5. If viscosity is temperature(volatile)-dependent there is a feedback that leads to self-regulation: temperature/volatiles increase → viscosity decreases → Ra increases & heat flow/degassing increase → temperature/volatiles decreases.

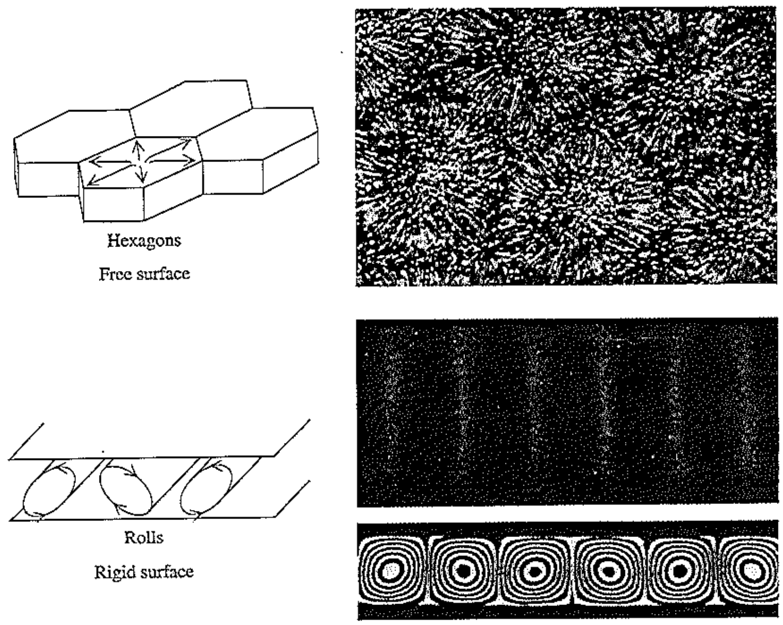

Figure 2

Two-dimensional rolls and three-dimensional hexagonal cells in a fluid layer heated from below, just above critical. (Bejan, 1995, Figure 5.22)

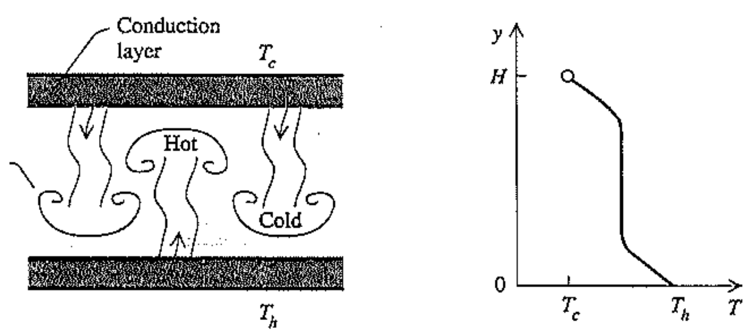

Figure 3

Isothermal convection, heated from below and cooled from above at high Rayleigh number. (Bejan, 1995, Figure 5.23)

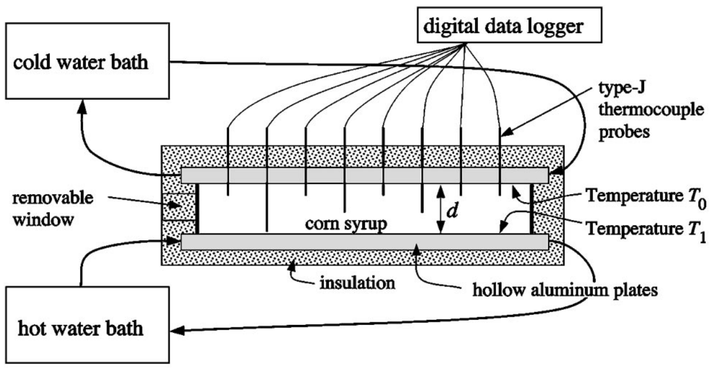

Figure 4

Figure 1 of Manga and Weeraratne, *Physics of Fluids*, 1999. Experimental apparatus.

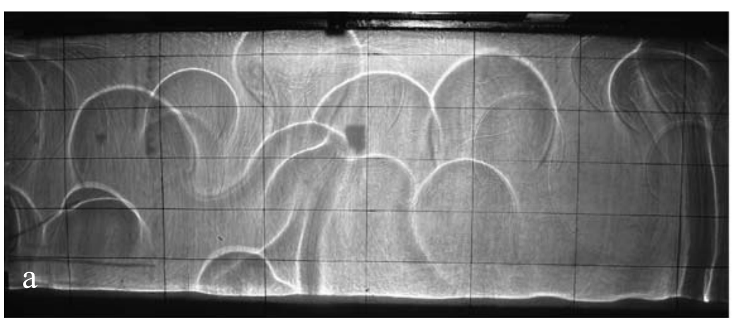

Figure 5

Figure 2 of Gonnermann et al., *Earth and Planetary Science Letters*, 2004. Shadowgraph image of convection with temperature-dependent viscosity at Ra $\sim 10^6$. Height approximately 0.5 m.

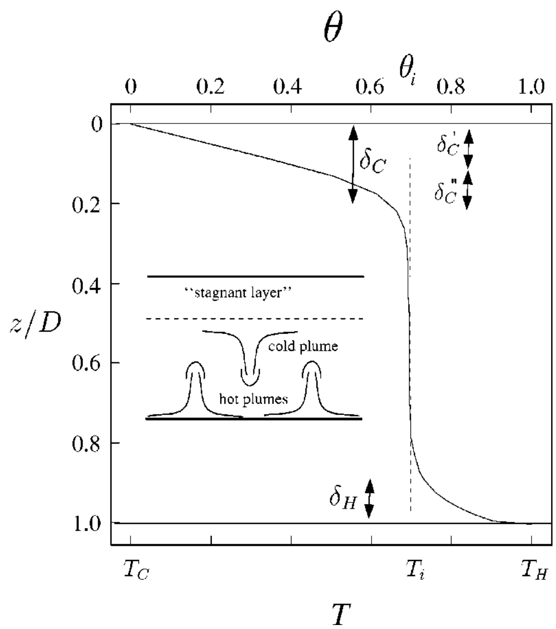

FIG. 1. Vertical temperature distribution; δ denotes boundary layer thicknesses, z is the vertical position, T is temperature, and θ is the dimensionless temperature.

Figure 6

Figure 1 of Manga et al., *Physics of Fluids*, 2001. Vertical temperature distribution during stagnant lid convection.

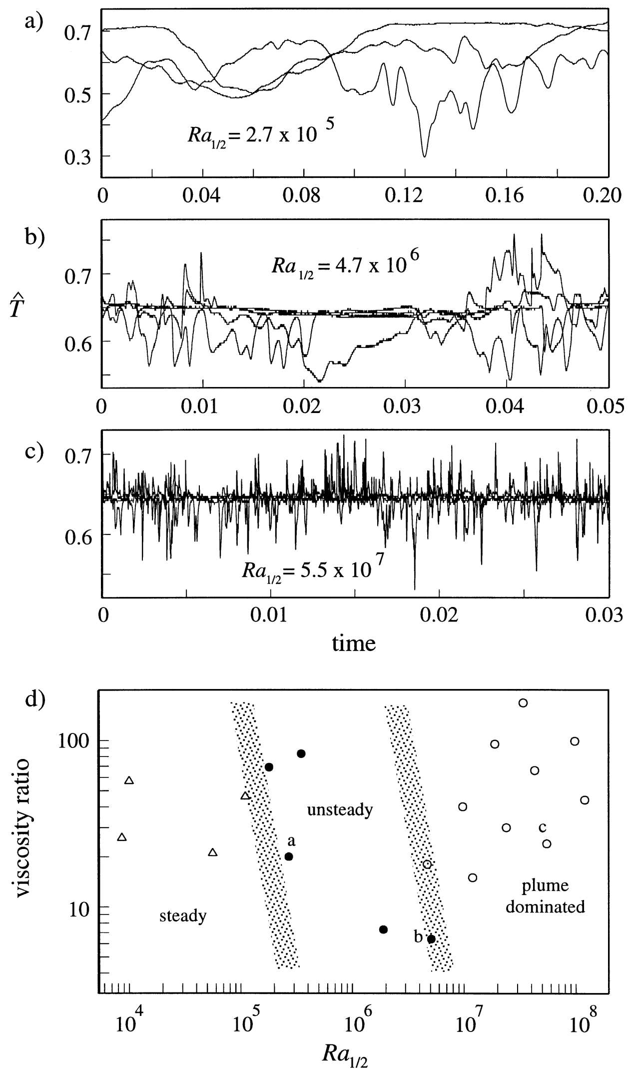

Figure 7

Figure 1 of Weeraratne and Manga, *Earth and Planetary Science Letters*, 1998. (a-c) Temperature as a function of time at different Rayleigh numbers. (d) Convective regimes.

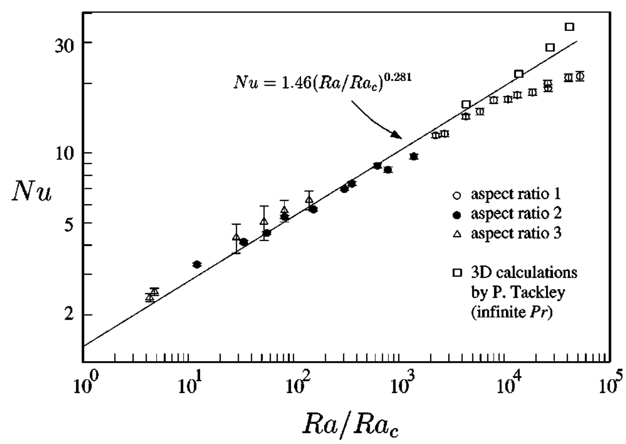

Figure 8

Figure 12 of Manga and Weeraratne, *Physics of Fluids*, 1999. Nu-Ra.

1.2. Conductive heat transfer

A FEW THINGS TO REMEMBER

1. Energy has units of J = N.m = kg.m^2/s^2.
2. Power has units of W = J/s = N.m/s = kg.m^2/s^3.
3. Heat flux, q, has units of W/m^2.
4. The specific heat capacity, c_p, has units of J/(K.kg).
5. Thermal conductivity, k, has units of W/(m.K).
6. Thermal diffusivity, $\alpha = k/(\rho c_p)$, has units of m^2/s.

Fourier's law of heat conduction in one dimension

$$q = -k\frac{dT}{dz} \tag{7.}$$

or more generally

$$q = -k\nabla T, \tag{8.}$$

where k is thermal conductivity in units of W m^{-1} K^{-1}, T is temperature and q is heat flux.

- What are the units of q?

From energy balance of a *representative elemental volume* it is possible to derive an equation for the conservation of energy for a solid or motionless fluid

$$\rho c_p \frac{\partial T}{\partial t} = -\nabla \cdot \mathbf{q}, \tag{9.}$$

where ρ is density and c_p is heat capacity. For constant material properties

$$\rho c_p \frac{\partial T}{\partial t} = k\nabla^2 T \tag{10.}$$

or

$$\frac{\partial T}{\partial t} = \alpha\nabla^2 T, \tag{11.}$$

where α is the thermal diffusivity (m^2 s^{-1}).

1.3. Nusselt-Rayleigh number from assumption of critically unstable thermal boundary layer

It should be noted that alternate derivations of the Nu-Ra scaling relation exist that result in relationships of Nu $\sim$ Ra$^{1/3}$. In fact, experiments show that measured convective heat fluxes fall somewhere between Nu $\sim$ Ra$^{1/4}$ and Nu $\sim$ Ra$^{1/3}$, depending on the magnitude of Ra, with the majority of experiments falling closer to Ra$^{1/3}$ than Ra$^{1/4}$. A very simple analysis is based on the following consideration.

A layer of fluid of thickness H, which is heated from below and cooled above begins to convect at Ra $\sim 10^3$. At Ra $> 10^3$, the layer convect in the form of two-dimensional rolls or hexagonal cells called *Bénard cells*. At Ra $\gg 10^3$, this orderly convection patter breaks down and the flow is by thermals or plumes. In this case the spatially averaged temperature in the interior of the layer is approximately uniform, with a cold and hot thermal boundary later (TBL) at the top and bottom, respectively. The TBL remains in a *critiacal state*, that is it thickens to the point of *instability*, where thermals or plumes are generated. This *critical thickness*, δ_T corresponds to the *critical Rayleigh number*, that is $\mathrm{Ra}_{\delta_T} \approx 10^3$, where

$$\mathrm{Ra}_{\delta_T} \equiv \frac{g\gamma \Delta T \delta_T^3}{\alpha\nu}. \qquad 12.$$

We can thus express the Rayleigh number for the layer in terms of Ra_{δ_T} as

$$\mathrm{Ra}_H = \mathrm{Ra}_{\delta_T}\left(\frac{H}{\delta_T}\right)^3 \sim 10^3\left(\frac{H}{\delta_T}\right)^3 \qquad 13.$$

and, hence,

$$\delta_T \sim 10\,H\,\mathrm{Ra}_H^{-1/3}. \qquad 14.$$

Because heat into and out of the convecting layer is by diffusion acorss the TBL, the actual heat flux is

$$q_{\text{convective}} \sim k\frac{\Delta T}{\delta_T}, \qquad 15.$$

whereas the conductive heat flux in the absence of convection would be

$$q_{\text{conducitve}} \sim k\frac{\Delta T}{H}. \qquad 16.$$

From this we obtain

$$\mathrm{Nu} \equiv \frac{q_{\text{convective}}}{q_{\text{conducitve}}} \sim \left(k\frac{\Delta T}{\delta_t}\right) / \left(k\frac{\Delta T}{H}\right) \sim \left(k\frac{\Delta T}{10\,H\,\mathrm{Ra}_H^{-1/3}}\right) / \left(k\frac{\Delta T}{H}\right) \qquad 17.$$

or

$$\mathrm{Nu} \approx 0.1\,\mathrm{Ra}_H^{1/3}. \qquad 18.$$

This result is rather remarkable, because it indicates that the thermal boundary layers are decoupled from the one another or the interior of the convecting layer. As H is increased conductive heat flow decreases, whereas convective heat flow remains constant. That this is so, can be seen by solving the $\mathrm{Nu} \sim \mathrm{Ra}^{1/3}$ relation for $q_{\text{convective}}$

$$q_{\text{convective}} \sim k\Delta T\left(\frac{g\gamma\Delta T}{\alpha\nu}\right)^{1/3}. \qquad 19.$$

Clearly, there is no dependence of $q_{\text{convective}}$ on H. It is, however, important to note that $\mathrm{Nu} \sim \mathrm{Ra}^{1/3}$ is a limit, and under a wide range of realistic conditions, especially at finite Pr where inertial forces may perhaps not be entirely negligible, it is found

$$\mathrm{Nu} = a\,\mathrm{Ra}^b, \quad \text{where} \quad \frac{1}{4} \le b \le \frac{1}{2}. \qquad 20.$$

1.4. Advanced considerations for Nusselt-Rayleigh number

As you can see, there seems to be some discrepancy in relationship between Nusselt number and Rayleigh number. Based on a large amount of experimental work, it turns out that there is no single relation that fits the Nusselt number for all values of Rayleigh number. Overall, it has been found that

$$\mathrm{Nu} = a\mathrm{Ra}^b. \qquad 21.$$

For example, the analysis from Section refsec:Nu-Ra-TurcotteSchubert gives

$$a = \mathrm{Ra}_c^{-b} \;\text{ and }\; b = 1/3, \tag{22}$$

where the critical Rayleigh number is $\mathrm{Ra}_c \approx 1000$. However, in reality constants a and b depend on the value of Ra and also on Pr. For example, Schubert et al. (*Mantle Convection in the Earth and Planets*, 2000) suggest that at very large Pr and Ra$= 10^6$

$$a = 0.27 \;\text{ and }\; b = 0.3185 \tag{23}$$

are good values. A recent comprehensive analysis by Grossmann and Lohse (*J. Fluid Mech.*, 2000) finds that across a wide range of Ra and Pr the following relationship is a reasonable approximation

$$\mathrm{Nu} = 0.27\,\mathrm{Ra}^{1/4} + 0.038\,\mathrm{Ra}^{1/3}. \tag{24}$$

Unfortunately, for earth scientists dealing with sub- and/or super-solidus convection in materials with a temperature dependent viscosity, the matter becomes more complicated. The thickness of the hot and cold thermal boundary layers is no longer equal and the average interior temperature is shifted to values somewhat greater than $(T_{\mathrm{cold}} + T_{\mathrm{hot}})/2$. Furthermore, it becomes more tricky to define the Rayleigh number, because viscosity is no longer a constant. One way this has been approached is outlined in Manga and Weeraratne (*Physics of Fluids*, 1999), where they defined the Rayleigh number based on the viscosity at $T = (T_{\mathrm{cold}} + T_{\mathrm{hot}})/2$, and obtained a Nu-Ra relationship of

$$\mathrm{Nu} = 1.46 \left(\frac{\mathrm{Ra}}{\mathrm{Ra}_c}\right)^{0.281} \tag{25}$$

for Ra $\lesssim 10^6$ and provided that Pr is sufficiently large.

1.5. Parameterized convection

The Nu-Ra scaling pertains to the steady heat transfer across a layer of fluid that is heated from below and cooled from above, by holding the temperatures at the top and bottom constant. Here we assume that this scaling applies to a convecting layer that is cooling, at a rate that is sufficiently slow, so that any given time the heat transfer from the layer can be obtained from the Nu-Ra relationship.

The rate of heat transfer out of a convecting layer of thickness H is

$$\rho c_p H A \frac{dT}{dt} = q_{\mathrm{convective}}\, A, \tag{26}$$

where A is surface area. Using Nu-Ra, we know that

$$q_{\mathrm{convective}} = a\,\mathrm{Ra}^b\, q_{\mathrm{conductive}} = \frac{a\,k\Delta T}{H}\mathrm{Ra}^b. \tag{27}$$

Therefore,

$$\frac{dT}{dt} = \frac{a\,\alpha\Delta T}{H^2}\,\mathrm{Ra}^b. \tag{28}$$

In the presence of internal heat generation Q (units of W m^{-3}) this equation becomes

$$\frac{dT}{dt} = \frac{a\,\alpha\Delta T}{H^2}\,\mathrm{Ra}^b + \frac{Q}{\rho c_p}. \tag{29}$$

For instantaneous heating or cooling of a half-space Turcotte & Schubert define thickness of the thermal boundary layer as that thickness over which the temperature changes by 90% of the temperature difference between the surface and the far field interior. Solving the heat equation using the similarity variable

$$\eta = \frac{z}{2\sqrt{\alpha t}}, \tag{30.}$$

where z is the spatial variable and $\sqrt{\alpha t}$ is the characteristic diffusion distance, gives for the heat flux at the surface

$$q = \frac{k\Delta T}{2\sqrt{\pi \alpha t}}, \tag{31.}$$

where the factor of 1/2 accounts for the fact that the temperature difference across the upper thermal boundary layer (the lithosphere) is $-\Delta T/2$. Assuming that the oceanic lithosphere is equivalent to a thermal boundary layer, Turcrotte & Schubert equate L to the thickness of the lithosphere as it cools with time, t, over which it has moved a distance $X = U_\mathrm{s} t$ from the spreading ridge. Here U_s is the spreading rate. The average residence time of oceanic lithosphere on the Earth's surface, τ, that is the average time before oceanic lithosphere subducts, is given by the area of the ocean floor $A_\mathrm{o} = A_\mathrm{E} - A_\mathrm{c}$, the total length of ridge, Y_r and the average spreading rate, U_s. We thus have

$$\tau = \frac{A_\mathrm{o}}{Y_\mathrm{r} U_\mathrm{s}}. \tag{32.}$$

Therefore the average heat flux at the surface of the oceanic lithosphere, $\bar{q}$ can be obtained from integration of Equation 31. as

$$\bar{q} = \frac{k\Delta T}{\sqrt{\pi \alpha \tau}}. \tag{33.}$$

Substituting for τ gives

$$\bar{q} = \frac{k\Delta T\sqrt{U_\mathrm{s}}}{\sqrt{\pi \alpha A_\mathrm{o}/Y_\mathrm{r}}}. \tag{34.}$$

Within the framework of our convective model, the convective heat flux $q_\mathrm{convective}$ equals the heat conducted through the upper thermal boundary layer (the oceanic lithosphere), that is

$$q_\mathrm{convective} = \hat{q} = k\frac{\Delta T}{2L}. \tag{35.}$$

Equating $\bar{q}$ with $q_\mathrm{convective}$ and solving for the spreading rate thus gives

$$U_\mathrm{s} = \frac{\pi \alpha A_\mathrm{o}/Y_\mathrm{r}}{(k\Delta T)^2} \cdot q^2_\mathrm{convective}, \tag{36.}$$

which is the same as Equation 45 of Tajika and Matsui (1992), except for the factor of 2 squared, due to the aforementioned definition of the temperature difference across the lithosphere.

TAKE-HOME MESSAGE

1. Using Nu-Ra one can calculate mantle temperature as a function of time.

2. This requires appropriate definition of the Ra and exponent b to account for internal heating and temperature/volatile-dependent viscosity and other 'complicating' factors.
3. Using Nu-Ra one can also calculate the MOR spreading rate, U_{r}.
4. In addition, Nu-Ra gives the depth of melting, d_{m}, beneath MORs, via mantle temperature (Section 3).
5. U_{r} together with d_{m} allow calculation of the melt production rate, which in turn is used to calculate the mantle degassing rate.

1.6. Internal heating

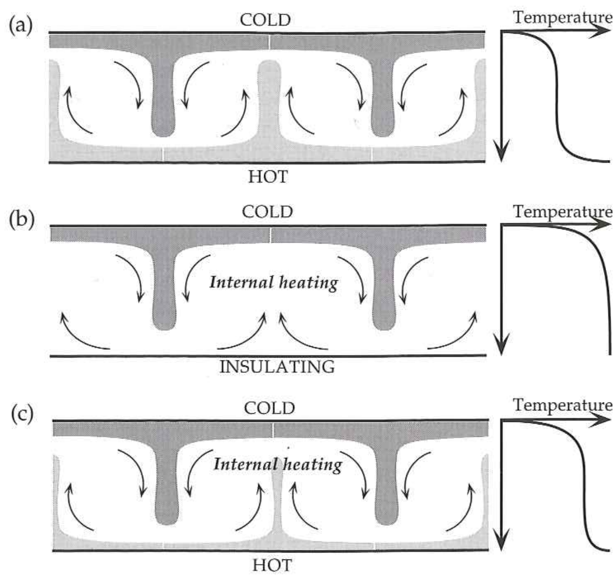

Figure 8.3. Sketches illustrating how the existence and strength of a lower thermal boundary layer depend on the way in which the fluid layer is heated.

Figure 9

Figure 8.3 of Davies.

2. MANTLE CONVECTION

2.1. Plate-scale and layered convection

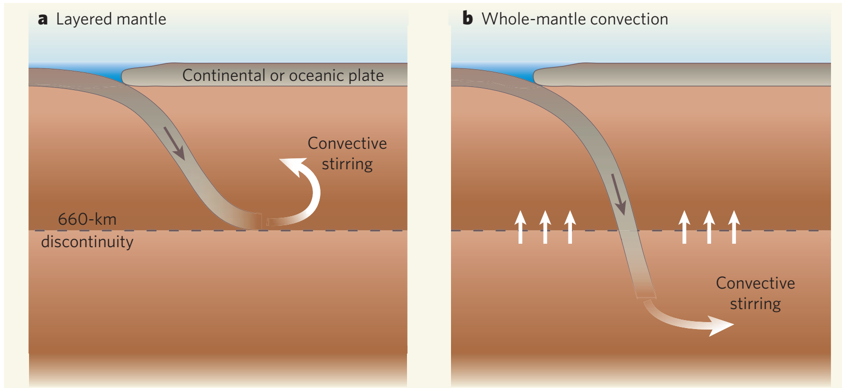

Figure 2 | The subduction connection. **a**, Models of noble-gas evolution have classically implied that only the upper mantle is effectively degassed[2,3], with the 660-kilometre seismic discontinuity producing a layered mantle by representing a boundary to the subduction of plates and the flow of material into the deep mantle. **b**, Seismological images[5], however, now provide strong evidence that plates can penetrate into the lower mantle, with the associated counterflow producing whole-mantle convection. The model of Gonnermann and Mukhopadhyay[1] shows that, contrary to many expectations, this mode of whole-mantle convection is quite compatible with observations of helium isotopes and other noble gases. Graphic not to scale.

Figure 10

Figure 2 of Elliott, Nature, 2009.

SUMMARY POINTS: PLATE-SCALE FLOW

1. The Earth has rigid plates, which in essence represent a cold, high-viscosity thermal boundary layer.
2. Plates can break and thereby move relative to each other and subduct. This is not the case for other planets, such as Mars or Venus.
3. When plates sink, they drive flow in the mantle at the spatial scale of plate tectonics. This length scale is larger than it would in the absence of plates.
4. Conservation of mass requires that the descending flow is balanced by (passive) ascending flow, some of which ultimately reaches the Earth's surface at mid-ocean ridges.
5. Plate motion is a consequence of negative buoyancy of the oceanic lithosphere. Plates are pulled at subduction zones (plate pull) and plates are pushed at ridges (ridge push). Which is the dominant force is somewhat controversial. These processes are reflected in the topography of oceanic lithosphere.

6. The presence of continental plates that cannot sink into the mantle complicates plate-scale convection.
7. The presence of phase transitions in the transition zone modulates plate-scale flow.
8. Increase in viscosity with depth in the lower mantle also modulates plate-scale flow.

SUMMARY POINTS: LAYERED MANTLE CONVECTION

1. Viscosity is thought to increase by a factor of 10-100 from upper to lower mantle. This result comes from the analysis of geoid anomalies.
2. Ocean-island basalts (OIBs) are isotopically distinct from mid-ocean ridge basalts (MORBs). MORBs are produced by melting of upper mantle. The mantle source of OIBs remains controversial, but they typically thought to originate in the lower mantle. This implies that there is considerable geochemical differences between upper mantle and OIB mantle reservoirs.
3. The transition zone can "retard" buoyant flow across it.
4. Small compositional changes (e.g., Fe, Si) between upper and lower mantle may translate to compositional density differences and convective stratification.
5. The combination of an increase in viscosity, transition zone, perhaps compositional density changes in conjunction with observed geochemical differences between OIBs and MORBs has led to the hypothesis of **layered mantle convection**.
6. Most numerical modeling of mantle convection suggests that layered mantle convection, if it exists at all, is "weak".
7. Seismic tomography indicates that slabs penetrate into the lower mantle, albeit not completely unfettered by the transition zone.
8. Alternative hypotheses for geochemical mantle heterogeneity are (1) that the mantle is heterogeneous at a small scale and that MORBs and OIBs are produced from different parts of the same heterogeneous mantle assemblage; (2) that OIBs originate from some ancient (primordial) layer, perhaps D", or some "stealth" mantle layer.

SOME COMPLICATING ISSUES

1. Mantle viscosity is temperature dependent.
2. Mantle viscosity depends on water content.
3. Internal heating affects Nu-Ra scaling.
4. Temperature-dependent viscosity can result in plume heads with persistent tails.
5. Mobile upper boundary vs. sluggish lid vs. stagnant lid.

SOME QUESTIONS

1. If slabs penetrate into the lower mantle mass balance requires that there is a return flow from lower mantle to upper mantle. Will this have led over Earth's history to complete homogenization of upper and lower mantle?

2. Where do OIBs originate?

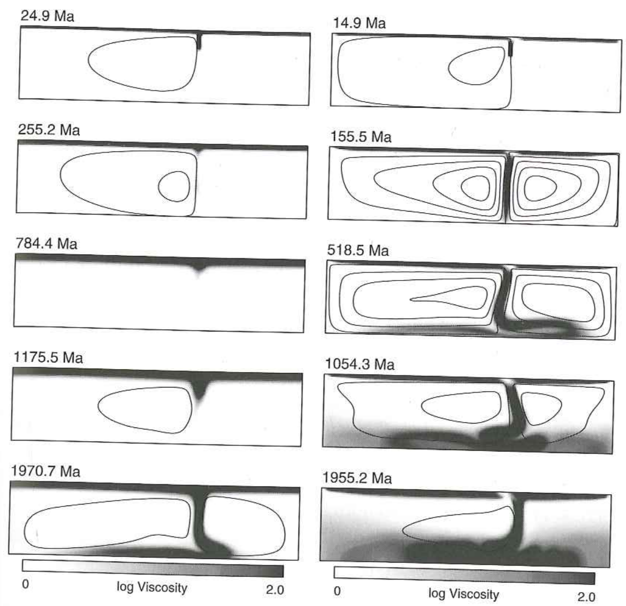

Figure 10.1. Numerical convection sequences. Left: with temperature-dependent viscosity (maximum viscosity 100 times the ambient viscosity). Right: the same with low-viscosity weak zones in the thermal boundary layer. The stiffness of the boundary layer inhibits the flow in the left sequence. The weak zones on the right allow pieces of the boundary layer to move more readily, simulating the motion of lithospheric plates. (Full technical specifications of this and subsequent numerical models are given in Appendix 2.)

Figure 11

Figure 10-1 of Davies. Plates are "weak" and "break" at plate boundaries. This changes the convective "planform".

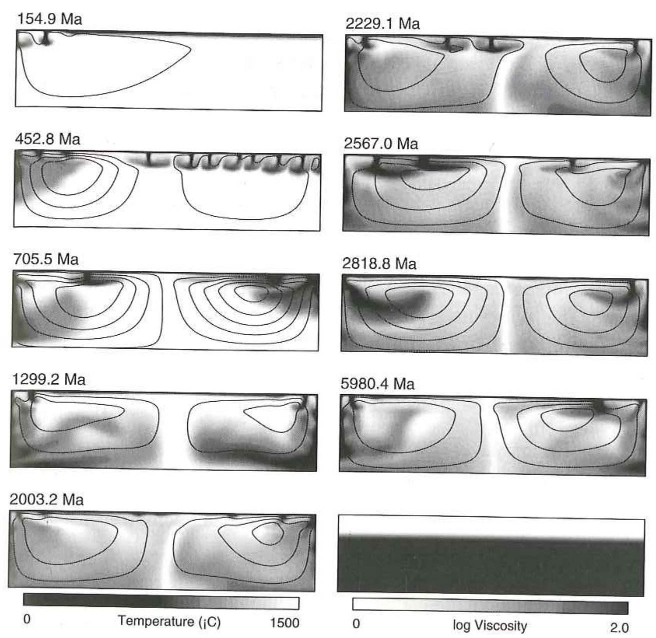

Figure 10.3. Convection sequence with layered viscosity and internal heating. The fluid in the lower part of the box has viscosity 100 times that in the upper part (lower right panel).

Figure 12

Figure 10.3 of Davies. Higher viscosity in the lower mantle decouples upper and lower mantle flow.

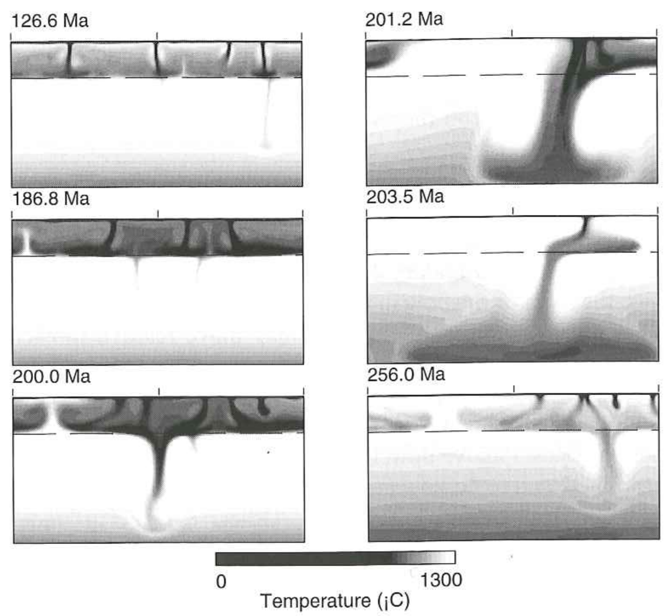

Figure 10.6. Constant viscosity convection sequence in which phase transformation buoyancy causes temporary layering of the flow. The buoyancy corresponds to a Clapeyron slope of $-3\,\mathrm{MPa/K}$. From [17]. Copyright by Elsevier Science. Reprinted with permission.

Figure 13

Figure 10.6 of Davies. Constant viscosity downwellings do not penetrate the transition zone, but instead pile up until sufficient thermally dense mass has accumulated to cause "overturn".

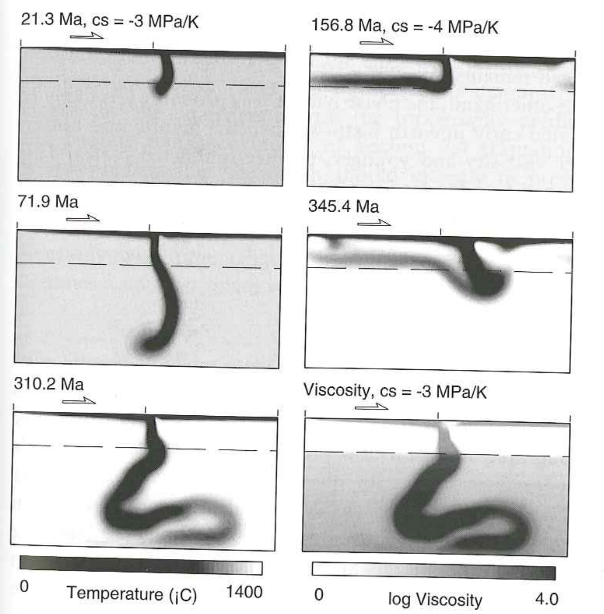

Figure 10.7. Convection sequences with a phase barrier and temperature-dependent viscosity, showing the greater ability of descending stiff sheets to penetrate a phase barrier than the constant-viscosity downwellings in Figure 10.6. Left: model with a Clapeyron slope (cs) of −3 MPa/K and reflecting end walls. The viscosity structure for the last frame is shown in the lower right panel. Right: Clapeyron slope of −4 MPa/K and periodic end walls, in which fluid that flows out at one end of the box flows back in at the other end. Penetration is delayed for a long time in the latter case. From [17]. Copyright by Elsevier Science. Reprinted with permission.

Figure 14

Figure 10.7 of Davies. If cold downwellings are of high viscosity, then they penetrate the transitions zone. This is even more accentuated in three-dimensions.

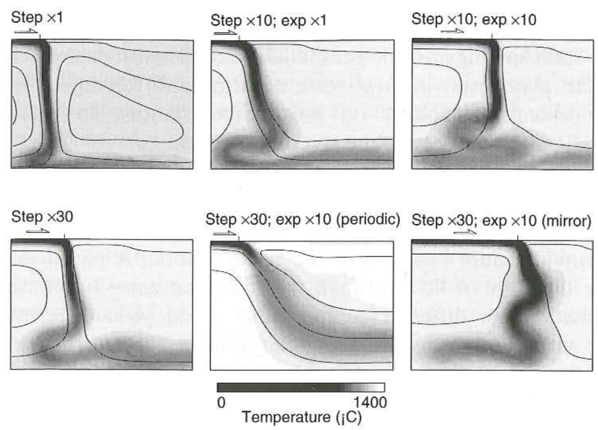

Figure 10.13. Frames from a series of convection models like that of Figure 10.12, with different variations of viscosity with depth. The cases are labelled with the magnitude of the viscosity step at 700 km and the magnitude of the superimposed smooth exponential increase, if any. The top left frame has no depth dependence. End boundary conditions are periodic, except in the lower right frame, which has no-flow ('mirror') end walls.

Figure 15

Figure 10.13 of Davies. Depth-dependent increase in viscosity causes plates to pile up and spread out in the lower mantle.

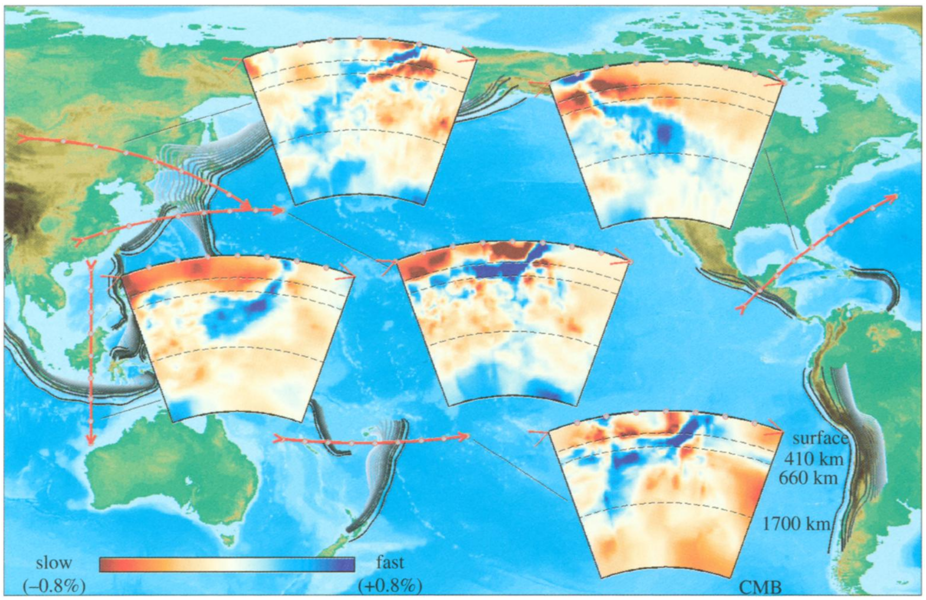

Figure 2. Series of mantle cross-sections through the recent P-wave model of Kárason & van der Hilst (2000) to illustrate the structural complexity in the upper-mantle transition zone and the regional variation in the fate of the slabs. Dashed lines are drawn at depths of 410, 660 and 1700 km, respectively. The model is based on short-period, routinely processed P, pP and PKP travel-time residuals (Engdahl *et al*. 1998) and a large number of PP-P and PKP-Pdiff differential times measured by waveform cross-correlation from long-period seismograms. The global model was parametrized with an irregular grid of constant-wave-speed cells, which allows high resolution in regions of dense data coverage, and three-dimensional finite frequency sensitivity kernels were used to account for different periods at which the measurements were made. With this technique, the low-frequency data can constrain long-wavelength mantle structure without preventing the short-period data from resolving small-scale heterogeneity.

Figure 16

Figure 2 of Albarede and van der Hilst (2002).

2.2. Plume-scale convection

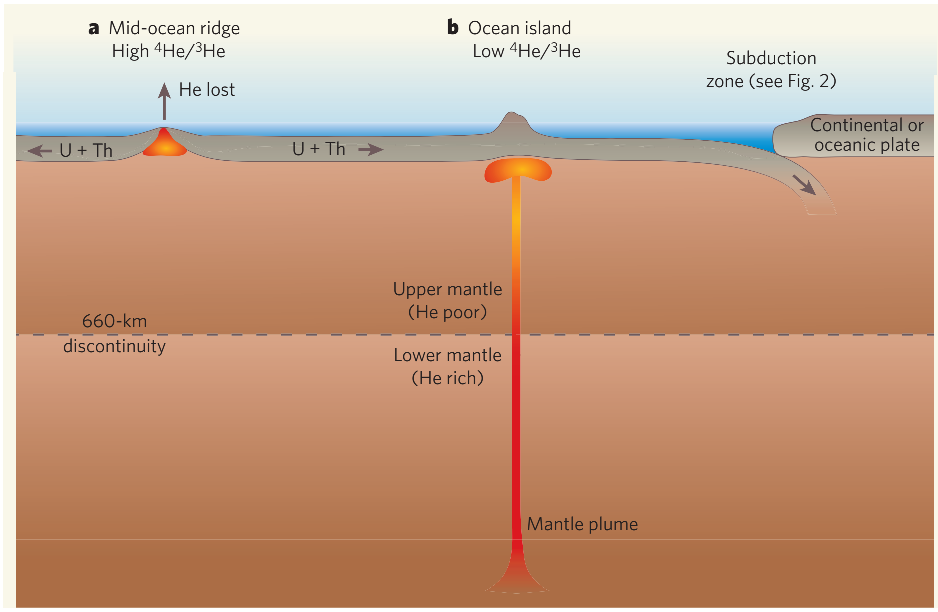

Figure 1 | Isotope ratios and Earth's mantle. **a**, As oceanic plates are pulled apart at mid-ocean ridges, the upper mantle rises in their place and (partially) melts. Uranium, thorium and helium in this portion of mantle are transferred to the magma, which migrates to the surface to form crust. Helium is lost during crystallization of the melts, but uranium and thorium are retained in the crust and are ultimately returned to the mantle by plate subduction (Fig. 2). Thus, the upper mantle becomes 'degassed' and the (U+Th)/He ratio increases, which with time translates into higher $^4He/^3H$ ratios. **b**, By contrast, ocean islands show a low $^4He/^3He$ ratio, thought to reflect a deep-mantle source of underlying mantle plumes. Graphic not to scale.

Figure 17

Figure 1 of Elliott, Nature, 2009.

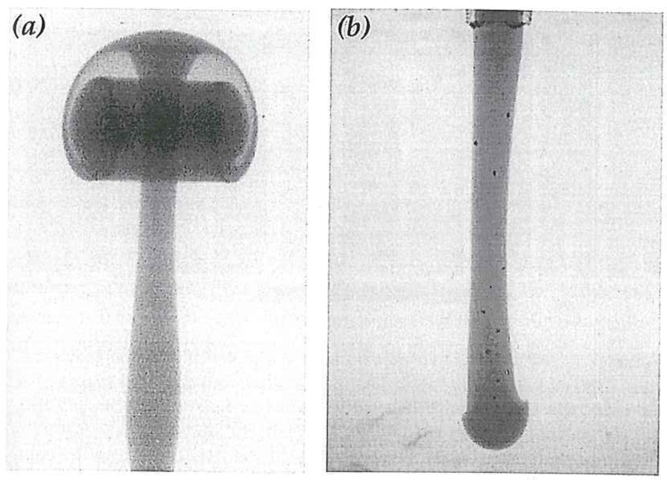

Figure 11.5. Thermal plumes in laboratory experiments, formed by injecting hot or cold dyed fluid into otherwise identical fluid. The fluid has a strong temperature dependence of viscosity. (a) The buoyant fluid is hot, and the plume viscosity is about 1/300 times that of the surrounding fluid. A spiral structure forms in the head due to thermal entrainment of ambient fluid. From Griffiths and Campbell [24]. (b) The injected fluid is cooler and hence denser and more viscous than the ambient fluid. There is little entrainment of cooled surrounding fluid, and only a very small head forms. From Campbell and Griffiths [25]. Copyright by Elsevier Science. Reprinted with permission.

Figure 18

Figure 11-5 of Davies.

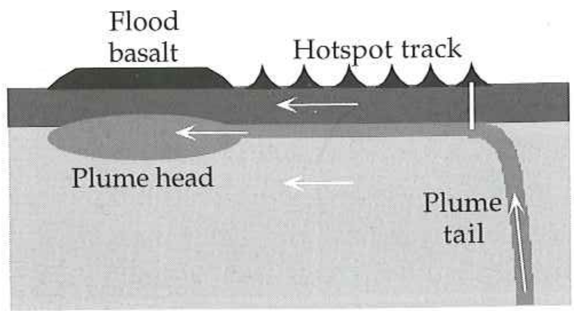

Figure 11.13. Sketch of the way a new plume with a head-and-tail structure can account for the relationship observed between some flood basalts and hotspot tracks, in which the hotspot track emerges from a flood basalt province and connects it to a currently active volcanic hotspot. It is assumed in the sketch that the plate and subjacent mantle are moving to the left relative to the plume source.

Figure 19

Figure 11-13 of Davies.

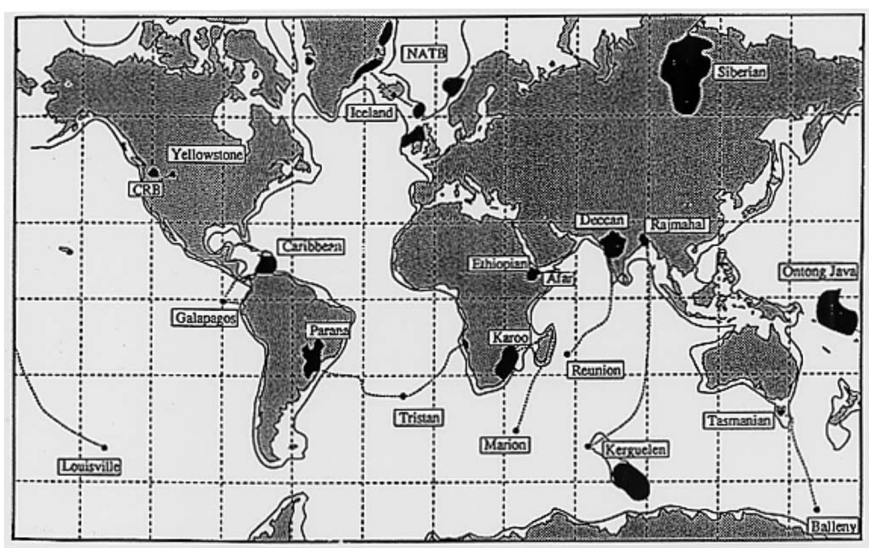

Figure 1. A map of hot spots that have both well-defined hot spot tracks and flood basalts at their origins [from *Duncan and Richards*, 1991].

Figure 20

Figure from Duncan and Richards, 1991.

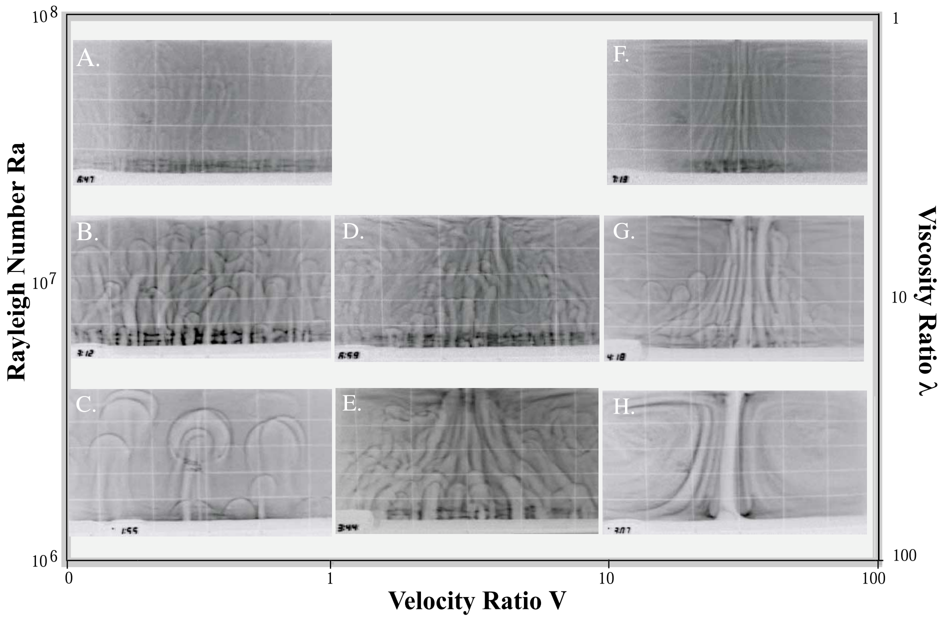

Figure 21

Figure 2 of Jellinek et al., EPSL, 2003.

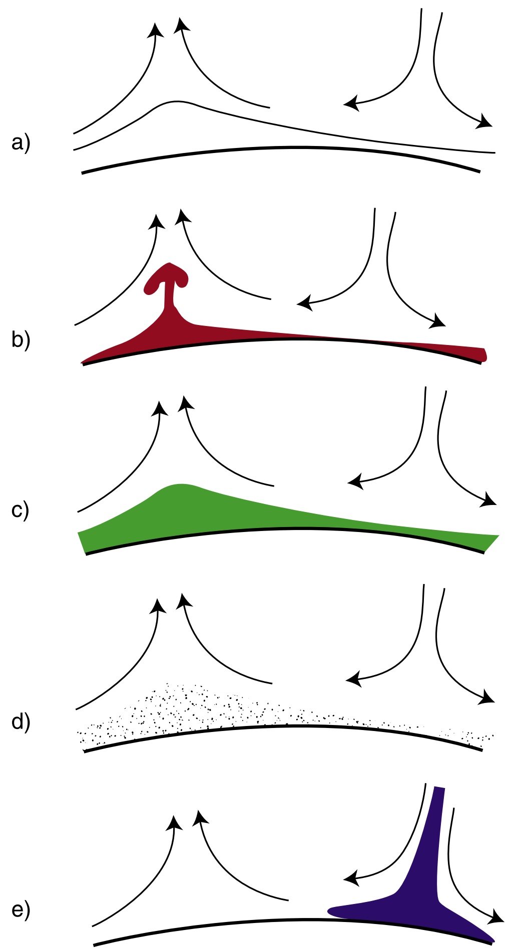

Figure 7. Schematic illustration of several models for D$''$. Within the context of plate tectonics, D$''$ has been explained variously as (a) a phase change, (b) a thermal boundary layer, (c) a compositional boundary layer, (d) ponded chemical dregs from subducted lithosphere, and (e) a slab graveyard.

Figure 22

Figure 7 of Jellinek and Manga, Rev. Geophys., 2004.

3. MELTING AT MORs

SUMMARY POINTS

1. Two-thirds of the Earth is resurfaced about every 100 million years. MOR spreading rates range from less than 10 mm yr^{-1} to nearly 200 mm yr^{-1}.
2. The *solidus* is the transition from complete solid to partial melt. Melting proceeds from 0% at the solidus to 100% several hundred degrees higher at the *liquidus*.
3. Hotter mantle results in more melt production and thicker ocean crust.
4. More melt production results in shallower depth to ridges.
5. Water will substantially increase the amount of melting beneath MORs. Each 0.1% of water added to the mantle lowers the solidus by 150 °C to 250 °C.

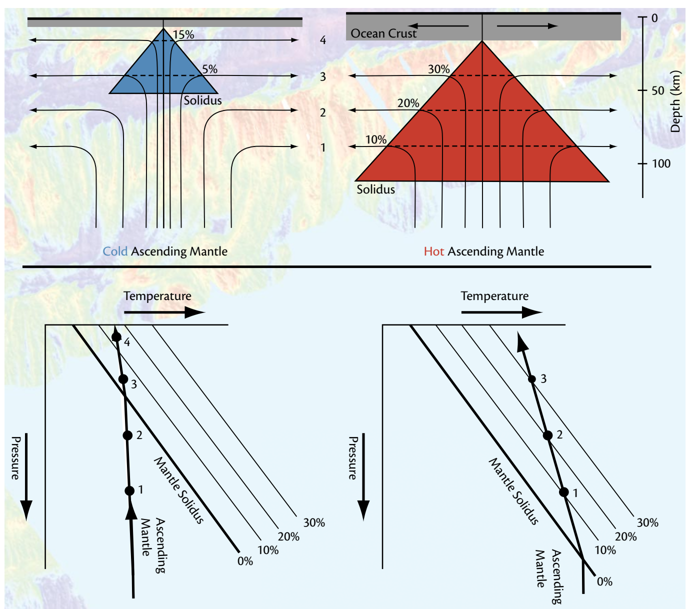

Figure 23

Figure 1. Diagrams illustrating the melting mechanisms beneath ocean ridges. At any one pressure, the mantle melts over a temperature range of several hundred degrees. e boundary between melt absent and melt present is called the mantle solidus. As mantle ascends beneath the ocean ridge, it begins melting as the solidus is crossed, and melts progressively dur- ing further ascent. us, the mantle melts by pressure decrease rather than by temperature increase. Hot mantle crosses the solidus at greater depths, leading to a larger melting regime, greater extents of melting, and thicker crust than that produced by cold mantle. e numbers on the bottom diagrams correspond to the pressures where melting stops for the numbered flow lines on the upper diagrams. (Langmuir & Forsyth, 2007, Figure 1).

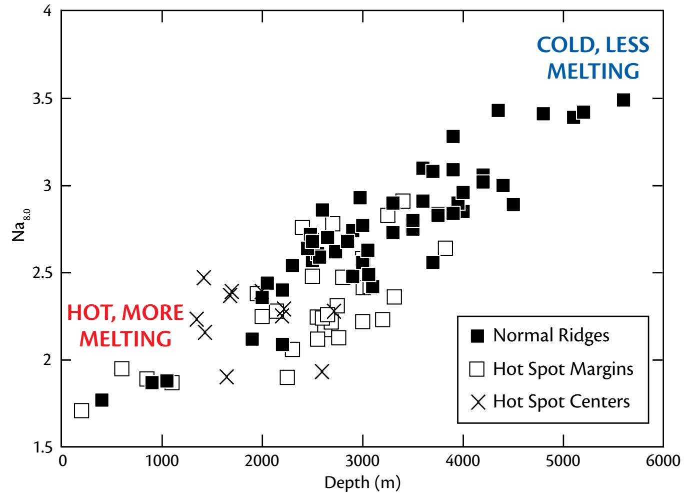

Figure 24

Figure 2. Plots of average compositions of ocean-ridge basalts (each point represents about 100 km of ridge length) vs. the average depth of the ridge. Na8.0 is the composi- tion of basalt normalized to a constant MgO content of 8 wt.% to correct for shallow- level differentiation. High Na contents reflect small extents of melting, while lower Na contents reflect higher extents of melting. High extents of melting lead to low Na con- tents, greater crustal thickness, and shallower depths below sea level, consistent with a model of varying mantle temperature. (Langmuir & Forsyth, 2007, Figure 2).

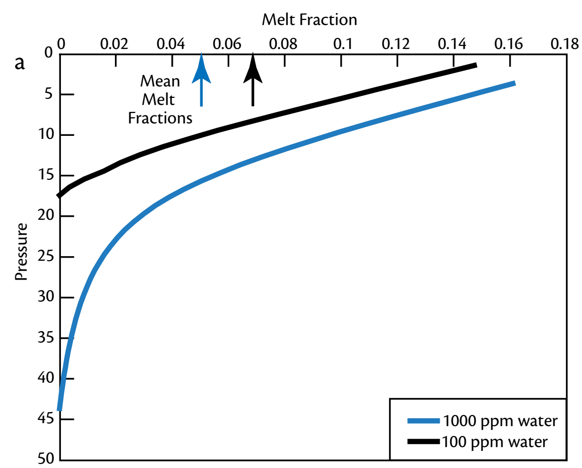

Figure 25

Figure 3. llustration of the effects of water on melting beneath ridges. Addition of water creates a deep 'tail' of low extents of melting, which contributes additional melt and causes greater crustal thickness. Although adding water causes the maximum extent and total amount of melt to increase, the average extent of melting across the whole depth of melting decreases because of the large, deep region of low-degree melts. (Langmuir & Forsyth, 2007, Figure 5a).

LITERATURE CITED

Langmuir & Forsyth, 2007. Langmuir CH, Forsyth DW. 2007. Mantle melting beneath mid-ocean ridges. *Oceanography* 20:78–89

Bejan, 1995. Bejan A. 1995. Convection Heat Transfer, 2nd Edition. *John Wiley & Sons, Inc., New York* pp. 623